Mon. Not. R. Astron. Soc. **000**, 000–000 (2001) Printed 1 February 2008 (MN LATEX style file v1.4)

Line-of-sight velocity distributions of low-luminosity elliptical galaxies

C. Halliday[1,4], Roger L. Davies[1], Harald Kuntschner[1], M. Birkinshaw[2], Ralf Bender[3], R.P. Saglia[3] and Glenn Baggley[1]

[1] *Department of Physics, University of Durham, Science Labs, South Road, Durham DH1 3LE, UK.*
[2] *H.H. Wills Physics Laboratory, University of Bristol, Tyndall Avenue, Bristol BS8 1TL, UK.*
[3] *Universitäts-Sternwarte, Scheinerstr. 1, D-81679 München, Germany.*
[4] *Current address: Astrophysics Research Institute, Liverpool John Moores University, Twelve Quays House, Egerton Wharf, Birkenhead CH41 1LD, UK. email: ch@astro.livjm.ac.uk*

Accepted — 2001. Received — ; in original form —

ABSTRACT

The shape of the line-of-sight velocity distribution (LOSVD) is measured for a sample of 14 elliptical galaxies, predominantly low-luminosity ellipticals. The sample is dominated by galaxies in the Virgo cluster but also contains ellipticals in nearby groups and low density environments. The parameterization of the LOSVD due to Gerhard and van der Marel & Franx is adopted, which measures the asymmetrical and symmetrical deviations of the LOSVD from a Gaussian by the amplitudes h_3 and h_4 of the Gauss-Hermite series. Rotation, velocity dispersion, h_3 and h_4 are determined as a function of radius for both major and minor axes. Non-Gaussian LOSVDs are found for all galaxies along the major axes. Deviations from a Gaussian LOSVD along the minor axis are of much lower amplitude if present at all. Central decreases in velocity dispersion are found for three galaxies. Two galaxies have kinematically-decoupled cores: NGC 4458 and the well-known case of NGC 3608.

Key words: galaxies: formation - galaxies: elliptical and lenticular - galaxies: kinematics and dynamics

1 INTRODUCTION

The shape and strength of absorption features provide a direct measure of the kinematics of integrated stellar populations in early-type galaxies (Sargent et al. 1977; Tonry & Davis 1979). Large format CCD arrays of small pixels enable two-dimensional studies of galaxy kinematics at high spectral and spatial resolution to be made using long-slit spectroscopy. This has led to the study of the line-of-sight velocity distribution (LOSVD) at different positions within a galaxy, allowing the kinematical structure to be tightly constrained (e.g., Franx & Illingworth 1988, hereafter FI88; Bender 1990, hereafter B90; Rix & White 1992, hereafter RW92; van der Marel & Franx 1993, hereafter vdMF93; Bender, Saglia & Gerhard 1994, hereafter BSG94, van der Marel et al. 1994, hereafter vdM94a, Fisher et al. 1995, hereafter F95, Statler & Smecker-Hane 1999, hereafter SSH99, Mehlert et al. 2000).

The orbital structure of a galaxy is a fossil record of its evolutionary history. However, there is a degeneracy between changes in mass-to-light ratio and velocity dispersion anisotropy that limits the analysis of rotation and dispersion measurements alone (Binney & Tremaine 1987). To recover the mass density distribution of a given galaxy requires at least an accurate determination of the velocity dispersion anisotropy through the LOSVD. A full determination of the galaxy dynamics would require the measurement of surface brightness profiles and is beyond the scope of this work but an accurate measurement of the LOSVD is an important step in achieving this (e.g., van der Marel et al. 1994, hereafter vdM94b; Saglia et al. 2000).

To a first approximation, elliptical galaxies are believed to be relaxed dynamical systems and the distribution of stellar velocities has been assumed to be Maxwellian producing approximately Gaussian profiles. However, within a number of ellipticals non-Gaussian LOSVDs have been measured. For example, see Figure 1 for LOSVDs measured in NGC 5582 at various radii. The non-Gaussian LOSVDs led to the detection of multiple component structures in ellipticals, such as kinematically-decoupled cores (FI88; Jedrzejewski & Schechter 1988, hereafter JS88), and central disks (RW92; van den Bosch et al. 1998). It has been demonstrated that under the assumption of Gaussian LOSVDs, the mea-

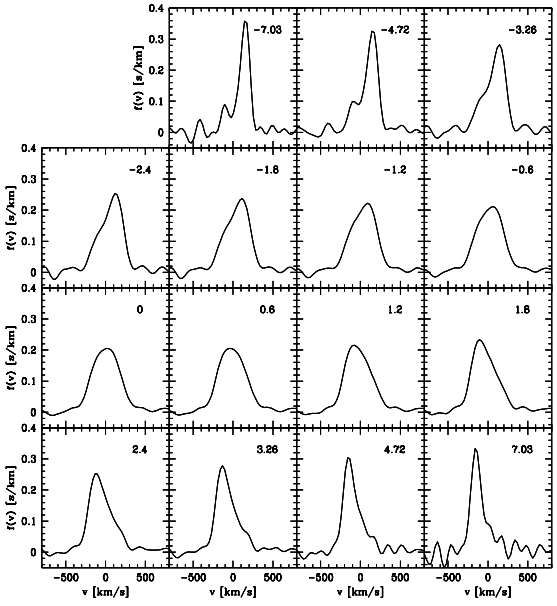

Figure 1. Recovered galaxy broadening functions for the major axis spectrum of NGC 5582. Radii of measurement are indicated in arcsec in each panel. The shape of the broadening function is clearly non-Gaussian for most of the radial bins. It is also evident how the width of the LOSVD increases towards smaller radii, in agreement with the larger measured values of the velocity dispersion σ.

surement of both rotation velocity and velocity dispersion can be incorrect by 10% or more (vdMF93).

To improve on the earlier measurements, more general parameterizations of the LOSVD have been tested and have been found to provide a superior description of the galaxy kinematical structure (RW92; vdMF93; Kuijken & Merrifield 1993; Zhao & Prada 1996). Here galaxy kinematics are measured using the Fourier Correlation Quotient (FCQ) method of B90. This method is considerably less sensitive to template-mismatching than traditional Fourier methods and allows the measurement of the full LOSVD. The LOSVD is then parameterized as a Gauss-Hermite series expansion (vdMF93) including the higher order terms h_3 and h_4.

The galaxy sample studied here consists mostly of low-luminosity ellipticals (hereafter LLEs). Evidence has grown steadily over the past 15 years that LLEs may be very different from the more luminous giant ellipticals, both in their kinematical behaviour (Davies et al. 1983, hereafter DEFIS83; Bender & Nieto 1990; Rix et al. 1999) and the properties of their stellar populations (e.g. Faber et al. 1992). As isotropic rotators (DEFIS83), LLEs are more easily modelled than the giant ellipticals which are believed to be supported by velocity dispersion anisotropy. Furthermore, the lower velocity dispersion broadening of LLEs enables the higher-orders of the LOSVD to be measured more accurately than for the more luminous ellipticals, provided that data of sufficiently high spectral resolution and signal-to-noise ratio (hereafter S/N) can be obtained.

The main objective of the measurements described here is to constrain the kinematical structure of our LLE sample as a function of radius. In Section 2, observations and reduction steps are described. The adopted LOSVD parameterization is presented and discussed in Section 3. A description of the measurement of galaxy kinematics using the FCQ method and measurements of rotation, σ, h_3 and h_4 are given in Section 4 and Appendix A. A short analysis of characteristic global kinematic parameters for the major axis of our sample is presented in Section 5 and a discussion of our results is given in Section 6. Comparisons between measurements obtained here and the measurements of previous authors are presented in Appendix B.

2 OBSERVATIONS AND BASIC REDUCTION

2.1 Galaxy Sample

A complete sample of 17 low-luminosity elliptical galaxies was selected from the Virgo catalog of Bingelli et al. (1985) covering the absolute magnitude range $-20 \leq M_B \leq -17$.

Nine galaxies of this original sample were observed. Other low-luminosity ellipticals (NGC 2778, NGC 3377, NGC 3605, NGC 3608, NGC 5582) were observed when Virgo was not available due to cloudy or windy conditions. The well studied 'bona fide' elliptical NGC 3379 was observed to enable consistency checks to be made with the measurements of other authors. Our observed sample is given in Table 1 which lists the morphological type, apparent magnitude B_T, the effective radius in arcsec (R_e), mean ellipticity, heliocentric redshift, cz_{helio} and environment. Values of absolute magnitude, as listed also in Table 1, were calculated using the distances from the surface-brightness-fluctuation survey of Tonry et al. (2001). Specifically we use a mean distance of 17.0 Mpc to the Virgo cluster, 11.1 Mpc to the Leo I group and 21.8 Mpc to the Leo II group. Two galaxies, NGC 2778 and NGC 5582, are in low density environments and we use the individual SBF distances of 16.9 Mpc and 28.4 Mpc, respectively.

2.2 Description of Observations

Long-slit spectroscopic data were obtained using the Blue Channel Spectrograph at the Multiple Mirror Telescope, Arizona, U.S.A., during 5-7 March and 15-17 May 1994, and 22-26 February 1995. The seeing varied from 0.5 to 2.0 arcsec. The Loral CCD detector of the Blue Channel Spectrograph was replaced between the observing runs of May 1994 and February 1995 with a chip of improved cosmetics. A summary of the instrumental set-up is given in Table 2.

A wavelength range of ∼4555-6045 Å was chosen to be centred on the Mg b, Fe5270 & Fe5335 Lick/IDS line-strength indices (Trager et al 1998). To accurately determine values of σ of as low as 60 km s^{-1}, a high spectral resolution of ∼1.5 Å FWHM was required; for this purpose a grating of 1200 g/mm and a slit width of 1 arcsec were used. The resolution element in the spatial direction was rebinned by 2 pixels to produce a spatial scale of $0\farcs6$ pixel^{-1}. The slit length was 180 arcsecs.

High S/N long-slit spectra were obtained for the major and minor axes of each galaxy of our sample. To determine kinematics 3-8 stellar template stars, predominantly G and K giants, were observed during each night. A log of all galaxy observations is given in Table 3: this includes the

Table 1. Observed Galaxy Sample

Name (1)	Type (2)	B_T (3)	R_e (4)	$\overline{\epsilon}$ (5)	cz_{helio} (6)	M_B (7)	environment (8)
NGC 2778	E	13.35	15.74	0.22	2019	-18.5	-
NGC 3377	E5+	11.24	34.45	0.48	692	-19.0	Leo I group
NGC 3379	E0	10.24	35.25	0.09	889	-20.0	Leo I group
NGC 3605	E4+	13.13	21.24	0.34	649	-18.6	Leo II group
NGC 3608	E2	11.70	33.66	0.21	1205	-20.0	Leo II group
NGC 4239	E	13.70	15.39	0.46	921	-17.5	Virgo
NGC 4339	E0	12.26	32.15	0.08	1281	-18.9	Virgo
NGC 4387	E	13.01	15.74	0.35	561	-18.1	Virgo
NGC 4458	E0+	12.93	26.13	0.13	668	-18.2	Virgo
NGC 4464	S?	13.46	7.54	0.24	1255	-17.7	Virgo
NGC 4467	E2	14.77	10.64	–	1474	-16.4	Virgo
NGC 4468	S0?	13.58	27.36	0.29	895	-17.6	Virgo
NGC 4478	E2	12.36	13.40	0.17	1382	-18.8	Virgo
NGC 4551	E	12.97	13.10	0.23	1189	-18.2	Virgo
NGC 4564	E6	12.05	19.82	0.58	1119	-19.1	Virgo
NGC 5582	E	12.48	32.89	0.32	1332	-19.8	-

Notes: Values of B_T in magnitudes, effective radius R_e in arcsec, and heliocentric redshift cz_{helio} in km s^{-1} were taken from the Third Reference Catalogue (de Vaucouleurs et al. 1991, hereafter RC3). The Hubble type, also taken from the RC3, is given in column 2: E-elliptical, S-spiral, S0-lenticular, +-intermediate (i.e. between elliptical and S0), ?-doubtful classification. Column 5 provides the mean ellipticity used in Section 5: these values were taken from Peletier et al. (1990), Bender et al. (1989) and Lauer et al. (1995); for NGC's 4239, 4339, 4458, 4468, 5582 values were obtained from the Digital Sky Survey. [a] To calculate the absolute magnitude M_B (column 7) we used the distances based on the surface-brightness-fluctuation survey of Tonry et al. (2001). Galaxies from Bingelli et al. (1985) that were contained in our original sample, but could not be observed are NGC 4168, NGC 4261, NGC 4360, NGC 4486A, NGC 4515, IC 3653, NGC 4623, NGC 4660. Column 8 indicates whether each galaxy is a member of the Virgo cluster, the Leo I group, the Leo II group or resides in a low density environment (-).

[a] The Digitized Sky Surveys were produced at the Space Telescope Science Institute under U.S. Government grant NAG W-2166.

Table 2. The instrumental set-up

Telescope	MMT
Instrument	MMT spectrograph, blue channel
Grating	1200 g/mm
Detector	Loral (3k×1k)
Pixel Size	15μm x 15μm
Readout Noise	$\sim 7-8$ e^-
Gain	~ 1.5 e^-/ADU
Slit width	$1''$
Spatial Scale	$0\farcs6$/pixel [a]
Instr. resolution	∼1.5 Å (FWHM)
Dispersion	0.5 Å/pixel
Wavelength range	4555 - 6045 Å

[a] binned 2× minimum bin size in spatial direction

date of observation, position angle (hereafter PA) of observation and the exposure time in seconds. Data for the galaxies NGC 4467 and NGC 4239 were of poor S/N and results for these objects will not be presented here.

Two different types of stellar observation were made: 'trailed' and 'rocked'. 'Trailed' spectra were obtained by trailing the stellar image along the length of the slit while the telescope was slightly de-focussed. A 'rocked' spectrum was created by moving the stellar image *across* the slit at regular intervals (10-20 arcsecs) along the slit length. This helped to ensure that the illumination of the slit and hence the instrumental broadening of observations, was identical for both star and galaxy spectra, and for this reason 'rocked' spectra were preferred for the kinematical analysis.

Exposures of both an incandescent lamp and the twilight night sky were obtained as flat-field standards. Standard He-Ar and Ne comparison lamp sources were observed simultaneously to enable wavelength calibration and geometrical rectification to be completed for all stellar and galaxy observations. For galaxy observations, comparison exposures were taken both before and after the exposure to monitor any shift in the instrumental set-up. For a given star, a single comparison exposure of ∼2-4 minutes was obtained for *both* the 'rocked' and 'trailed' exposures where these were taken consecutively.

2.3 Basic Reduction

A standard data reduction was performed principally using IRAF ⋆. To complete the measurement of galaxy kinematics additional steps were performed using IRAF and MIDAS †.

Reduction steps, performed for each night of observation, are summarized; for a more detailed description see

⋆ Image Reduction and Analysis Facility of the National Optical Astronomy Observatories, Tuscon, Arizona, U.S.A..

† Munich Image Data Analysis System of the European Southern Observatory.

Table 3. Observing Log

Date (1)	Name (2)	PA (deg.) (3)	Exp. (s) (4)
05.03.94	NGC 3605	290 min	3600
05.03.94	NGC 3605	200 maj	3600
05.03.94	NGC 4387	322 maj	3600
05.03.94	NGC 4387	52 min	3600
05.03.94	NGC 4564	135 min	3600
05.03.94	NGC 4468	155 min	3600
06.03.94	NGC 3608	351 min	3600
06.03.94	NGC 2778	225 maj	3600
06.03.94	NGC 2778	135 min	3600
06.03.94	NGC 5582	205 maj	3600
15.05.94	NGC 4564	45 maj	3600
15.05.94	NGC 4468	65 maj	3600
15.05.94	NGC 4464	95 min	3600
15.05.94	NGC 4464	5 maj	3600
15.05.94	NGC 5582	295 min	4200
16.05.94	NGC 3608	81 maj	3600
22.02.95	NGC 4467	41 maj	3600
22.02.95	NGC 4467	131 min	3600
23.02.95	NGC 3379	71 maj	600
23.02.95	NGC 3379	161 min	600
23.02.95	NGC 3377	42 maj	1800
23.02.95	NGC 3377	312 maj	1800
23.02.95	NGC 4551	70 maj	3600
23.02.95	NGC 4551	340 min	3600
23.02.95	NGC 4458	5 maj	3600
23.02.95	NGC 4458	95 min	3600
23.02.95	NGC 4478	145 maj	3600
24.02.95	NGC 4478	55 min	3600
24.02.95	NGC 4339	20 maj	2700
24.02.95	NGC 4339	110 min	2700
24.02.95	NGC 4239	115 maj	5400

Notes: The date of each observation and galaxy name is given in columns 1 & 2, respectively. Column 3 gives the position angle of the observation with sense North through East; positions corresponding to the major (maj) and minor (min) axes are indicated. Column 4 lists the exposure time in seconds.

Halliday (1998). All CCD observations were bias-subtracted, flat-fielded and corrected for the effects of both cosmic ray hits and bad pixel columns. A wavelength calibration was performed for each star and galaxy frame to a typical accuracy of 0.05 Å ($\sim$ 3 km s^{-1} at $\sim$5200 Å). A series of distortion maps were created to geometrically rectify each frame to a typical accuracy of 0.2 pixels RMS ($\sim$6 km s^{-1} at $\sim$5200 Å). Background sky signal was subtracted for each galaxy frame by linearly-interpolating between areas of sky at opposite sides of the galaxy spectrum. A correction for chromatic focus variations within a galaxy frame was made where required. This involved measuring the central width of the galaxy profile as a function of wavelength. A procedure was developed to smooth the galaxy profile width to the same value for all wavelengths. This was similar to a procedure adopted by Mehlert et al. (1998) to correct for chromatic focus variations detected within their data. The dispersion axis of each galaxy frame was finally rebinned on to a natural logarithmic scale.

A one-dimensional stellar spectrum was created for each 'rocked' star frame by extracting individual 'strips' of spectra within each frame. These were combined to produce a single one dimensional spectrum and deredshifted to laboratory wavelengths.

3 PARAMETERIZATION OF THE LINE-OF-SIGHT VELOCITY DISTRIBUTION

The line-of-sight velocity profile was decomposed using the parameterization proposed by Gerhard (1993) and van der Marel and Franx (1993):

$$f(y) = I_0 e^{-\frac{y^2}{2}}(1 + h_3 H_3(y) + h_4 H_4(y)) \quad (1)$$

where $y = \frac{(\nu_{fit} - \nu)}{\sigma_{fit}}$, ν_{fit} is the measured velocity; ν is the mean of all measured velocities for a given spectrum (i.e., the mean radial velocity); σ_{fit} is the measured velocity dispersion; $H_3(y)$ and $H_4(y)$ are antisymmetric and symmetric standard Gauss-Hermite polynomials of 3rd and 4th order and h_3 and h_4 are their coefficients, respectively; and I_0 is a normalization constant.

The coefficient h_3 quantifies the LOSVD asymmetry. Measured asymmetries for elliptical galaxies arise from a non-Gaussian velocity distribution along the line-of-sight, e.g., the superposition of a slowly rotating bulge and a more rapidly rotating disk component. Positive measurements of h_3 correspond to a distribution skewed towards velocities *lower* than the measured systemic velocity of the galaxy. Conversely negative h_3 measurements correspond to distributions skewed towards velocities greater than the systemic velocity.

The h_4 term quantifies the symmetric deviations of the LOSVD from a Gaussian. For $h_4 > 0$ the corresponding distribution is more peaked than a Gaussian at small velocities with more extended high velocity tails. Conversely, distributions less peaked than a Gaussian will have $h_4 < 0$.

4 GALAXY KINEMATICS: MEASUREMENT AND RESULTS

Measurements of rotation, σ, h_3 and h_4 were obtained using the FCQ method of B90. This procedure involved extraction of an appropriate wavelength range, binning the spectra as a function of radius to a particular value of S/N, continuum level removal and application of a Wiener filter.

Optimal values of parameters for each of the measurement steps were established using Monte-Carlo simulations. Simulated 'galaxy' spectra for particular measurements of σ, h_3 and h_4 were created from one-dimensional stellar spectra. To model the effect of noise in simulations for a given S/N, different Gaussian noise realisations were added to 30 copies of each simulated galaxy spectrum. The mean value and spread of kinematical measurements obtained for the different spectra were used to determine the optimal value for each parameter (for details see Halliday 1998).

From our overall wavelength range, we extracted a range centred on the Mg b spectral feature and excluding Hβ. Galaxy spectra were rebinned in the direction of the spectroscopic slit to a minimum signal-to-noise ratio (S/N) of 60 per Å and separately for S/N = 30 per Å. The shapes

of continuua were removed for the stellar and galaxy spectra by fitting and dividing by a third order polynomial. The edges of all spectra were tapered using a cosine bell function. Filtering of high frequency noise was performed using an appropriate Wiener filter. Error estimation involved the calibration of the peak-to-noise ratio of the power-spectrum of the galaxy spectra with the value of the signal-to-noise ratio. Simulations of galaxy spectra at different radii were performed to derive their signal-to-noise ratio and therefore the error values.

Measurements were obtained for 3-8 different stellar templates. Only templates observed on the same night of observation were used for a given galaxy; this is important since a central assumption of the FCQ method is that the instrumental broadening of the galaxy and stellar spectra can be assumed to be similar. Although the FCQ method reduces the effect of template-mismatching, measurements of the higher order terms h_3 and h_4 are still sensitive to spectral differences between template star and galaxy. For an elliptical galaxy of axisymmetric kinematical structure, where the spectroscopic slit has been carefully centred on the galaxy centre, the h_3 profile is expected to have reflection symmetry about the galaxy centre. Template-mismatching produces a constant offset in h_3. The final template was choosen to minimize the offset in h_3. Where possible, identical templates were used to derive measurements for the major and minor axis spectrum of each galaxy. Where major and minor axis observations were obtained on different nights and identical templates could not be used, templates of most closely matching stellar type were chosen.

In Appendix A we present measurements of rotation, σ, h_3 and h_4 for the major and minor axes of our sample galaxies. A range of different kinematical behaviour is evident. Significant LOSVD asymmetries are measured for 13 out of 14 galaxies along the major axis. Central dips in σ are measured for the major and minor axis of three galaxies. Two galaxies are found to have kinematically-decoupled cores.

5 CHARACTERISTIC KINEMATICAL PARAMETERS

In this section characteristic, global kinematic parameters are derived and analysed for the major axes of each galaxy. Six parameters were determined for each individual galaxy: v_{max} the maximum measured rotation velocity; σ_0, σ_{max} and $\overline{\sigma}$, the central, maximum and mean velocity dispersion, respectively. For $\overline{\sigma}$, values were taken to be the mean of all measurements within $\frac{1}{2}\mathrm{R}_e$. Furthermore $\overline{|h_3|}$, the mean of the absolute values of h_3, and $\overline{h_4}$, the mean value of h_4 were determined. For $\overline{|h_3|}$ and $\overline{h_4}$, the mean of all measurements within $\frac{1}{2}\mathrm{R}_e$, excluding the innermost measurements ($|r| \lesssim 2\farcs6$), was taken. Uncertainties were calculated by propagating the errors determined for the original measurements of rotation, σ, h_3 and h_4. A summary of all values is given in Table 4.

In Figure 2 the ratio of v_{max} to the mean velocity dispersion $\overline{\sigma}$ is plotted against the mean ellipticity $\overline{\epsilon}$. Predictions for an oblate isotropic rotator model from Binney (1978) are shown as a solid line. These predictions were obtained using the tensor virial theorem, assuming constant ellipticity. Measurements obtained here for the low luminosity ellipticals are found close to the predictions for isotropic rotators with the exception of NGC 5582. The latter galaxy shows unusually strong rotation for its mean ellipticity. Our data is in good agreement with the earlier findings of DEFIS83 (their LLEs are shown as open triangles in Figure 2).

The deviations from a Gaussian LOSVD as measured by the higher order terms h_3 and h_4, span a large range in values within and between galaxies. The mean values of $\overline{|h_3|}$ vary from $+0.013$ to $+0.169$ between galaxies, and $\overline{h_4}$ varies from -0.060 to $+0.104$. The largest values of h_3 and h_4 are detected in NGC 5582. We did not find clear correlations between our global parameters and the higher order terms h_3 and h_4. However, two interesting diagrams concerning h_3 are shown in Figure 3.

In Figure 3(a) the ratio of v_{max} to $\overline{\sigma}$ is plotted against $\overline{|h_3|}$ for each galaxy. We note that there is a weak trend such that galaxies with larger ratios of $v_{max}/\overline{\sigma}$ have on average larger values of $\overline{|h_3|}$. This suggests that greater rotational support may be related to larger LOSVD asymmetries. In Figure 3(b) it is shown that the largest values of $\overline{|h_3|}$ are measured for galaxies with intermediate values of σ_0. LOSVD asymmetries may be more common for these galaxies. A larger sample is needed to confirm this suggestion.

6 DISCUSSION

We have demonstrated in Section 5 that for our sample of LLEs the *global* kinematic parameters such as v_{max}, $\overline{\sigma}$ and $\overline{\epsilon}$ are consistent with the predictions for a simple oblate isotropic rotator model.

In general, however, we find a wide range of complex kinematical behaviour in our sample. There is a wide range of velocity dispersion gradients with radius. Some galaxies, such as NGC 3377, show a steep decline, whereas others, such as NGC 4551, have a rather shallow profile. Central decreases in σ are measured for three galaxies for the major and minor axes (NGC 4387, NGC 4478 and NGC 4551), and two galaxies (NGC 3608 and NGC 4458) are found to have kinematically-decoupled cores (KDCs). Significant asymmetric line-of-sight velocity distributions, parameterized by the Gauss-Hermite coefficient h_3, are measured for 13 low-luminosity ellipticals. These asymmetries are found mainly for radii close to the galaxy centre, and suggest that we are detecting the motion of two or more components of different kinematical properties in at least some of the low-luminosity ellipticals.

The LOSVDs along the minor axis are generally consistent with a Gaussian shape. Only a few galaxies show significant h_3 or h_4 terms. In the cases where non-Gaussian LOSVDs are detected this can be explained by isophote twisting such that our slit does not follow the exact location of the kinematic minor axis. This may also explain the non-zero velocities measured for some galaxies along the minor axis (e.g, NGC 3377 and NGC 4464). NGC 4478 is the most spectacular case, since it exhibits signs of disturbed, perhaps unrelaxed kinematics. This galaxy is not axisymmetric and any dynamical model would need to be triaxial. This is also likely to be the case for the other galaxies which show non-zero velocities along the minor axis.

Table 4. Global parameters

Name (1)	v_{max} (2)	dv_{max} (3)	σ_{max} (4)	dσ_{max} (5)	σ_0 (6)	dσ_0 (7)	$\overline{\sigma}$ (8)	d$\overline{\sigma}$ (9)	$\overline{\lvert h_3 \rvert}$ (10)	d$\overline{\lvert h_3 \rvert}$ (11)	$\overline{h_4}$ (12)	d$\overline{h_4}$ (13)
NGC 2778	109.4	9.3	169.2	1.0	168.7	0.9	142.1	0.6	0.078	0.008	0.028	0.009
NGC 3377	100.1	0.9	156.0	1.8	156.0	1.8	101.6	0.5	0.124	0.006	-0.035	0.009
NGC 3379	50.0	5.7	224.5	2.8	221.1	2.9	209.5	1.3	0.025	0.009	-0.001	0.010
NGC 3605	55.9	8.5	91.9	0.6	90.8	0.5	87.6	0.2	0.042	0.005	0.002	0.005
NGC 3608	45.4	5.2	201.6	0.8	201.6	0.8	179.3	0.4	0.034	0.003	0.016	0.003
NGC 4339	56.3	5.4	115.2	1.0	115.2	1.0	100.4	0.5	0.072	0.007	0.081	0.010
NGC 4387	59.8	7.4	101.4	0.9	97.9	0.6	97.1	0.3	0.013	0.003	0.009	0.004
NGC 4458	26.3	1.2	119.0	2.1	119.0	2.1	97.8	0.7	0.059	0.013	-0.035	0.018
NGC 4464	78.0	1.2	141.2	0.6	141.2	0.6	120.9	0.4	0.150	0.007	0.051	0.008
NGC 4468	24.2	2.9	36.2	1.6	34.6	1.2	33.2	0.8	0.029	0.043	-0.060	0.027
NGC 4478	58.4	3.1	146.0	3.7	126.3	2.0	131.7	0.8	0.054	0.007	-0.014	0.008
NGC 4551	46.6	2.0	103.5	1.2	103.5	1.2	95.2	0.4	0.053	0.005	-0.034	0.008
NGC 4564	153.2	1.6	177.4	0.4	177.4	0.4	144.8	0.2	0.027	0.002	-0.016	0.002
NGC 5582	165.2	10.0	164.6	0.7	164.6	0.7	125.8	0.5	0.169	0.007	0.104	0.010

Global parameters, as plotted in figures 2 and 3, are given for the major axis spectrum of each galaxy. Columns 2 & 3 give the maximum measured rotation velocity and its error. The maximum, central and mean velocity dispersion and their corresponding errors are given in columns 4 & 5, 6 & 7 and 8 & 9, respectively. Columns 10 & 11 give the mean absolute value of h_3 and its error. The mean value of h_4 and its error are given in columns 12 & 13. All measurements of velocity and σ are given in km s^{-1}.

Some of the kinematic signatures we detect in our sample of LLEs, such as KDCs and central dips in velocity dispersion, are indicative of a merger scenario. It is interesting to note that in their recent merger simulations, Bendo and Barnes (2000, hereafter BB2000) have presented LOSVDs for the merger remnants of two spiral galaxies, which resemble elliptical galaxies. In these simulations central dips in σ were found for remnants of an *equal-mass* merger of two spirals. Predictions for the profiles of rotation, h_3 and h_4 are however different from those observed in our study. In most cases h_3 is predicted to have a similar sign to the rotation velocity close to the galaxy centre; for our galaxy sample, h_3 has an *opposite* sign to rotation. In one case in the study of BB2000, where h_3 and rotation do have opposite signs, the merger remnant has a counterrotating core: neither of the two galaxies in our sample with a counterrotating core (i.e. NGC 3608 and NGC 4458) have a central decrease in σ. For NGC 4387, rotation rises steadily outside the galaxy centre in agreement with the simulation results, although h_4 is consistent with zero in contrast to the predicted values of positive h_4. Rotation velocities for the unequal-mass mergers considered by BB2000 are of far greater amplitude than the velocities measured in this study.

Our long-slit observations provide a valuable insight into the dynamics of LLEs and demonstrate clearly that there exists a wide range of complex, sometimes non-axisymmetric kinematics. With data available only for the major and minor axis of a galaxy it is difficult, if not impossible, to describe the full dynamical make-up of galaxies. The newly commisioned integral field units such as SAURON (Bacon et al. 2001), however, provide 2-dimensional rotational velocity and velocity dispersion maps of early-type galaxies and will advance this area of astronomy.

7 ACKNOWLEDGEMENTS

We thank the CFA Observing Time Committee for their generous allocation of telescope time. CH thanks Frank van den Bosch for kindly providing his photometric measurements for NGC 4478 and NGC 4564. CH acknowledges helpful discussions with Reynier Peletier and the support of a PPARC studentship at the University of Durham and a PPARC PDRA grant at Liverpool JMU. HK was supported at the University of Durham by a PPARC rolling grant in Extragalactic Astronomy and Cosmology.

REFERENCES

Bacon, R., et al., 2001, MNRAS, submitted
Bender, R., Surma, P., Döbereiner, S., Möllenhoff, C., Madejsky, R., 1989, AA, 217, 35
Bender, R., 1990, AA, 229, 441 (B90)
Bender, R., Saglia, R. P., Gerhard, O. E., 1994, MNRAS, 269, 785 (BSG94)
Bendo, G. J., Barnes, J. E., 2000, MNRAS, 316, 315 (BB2000)
Binney, J., 1978, MNRAS, 183, 501
Binney, J., Tremaine, S., 1987, Galactic Dynamics, Princeton University Press
Binggeli, B., Taummann, G., Sandage, A., 1985, AJ, 90, 1681
Carollo, C. M., Franx, M., Illingworth, G. D., Forbes, D. A., 1997, ApJ, 481, 710 (C97)
Carter, D., 1987, ApJ, 312, 514
Davies, R. L., Efstathiou, G., Fall, S. M., Illingworth, G., Schechter, P. L., 1983, ApJ, 266, 41 (DEFIS83)
de Vaucouleurs, G., de Vaucouleurs, A., Corwin, H. G. J., Buta, R. J., Paturel, G., Fouqué, P., 1991, Third Reference Catalogue of Bright Galaxies. Springer Verlag (RC3)
Faber, S. M., Worthey, G., Gonzales, J. J., 1992, IAU Symp. 149, The Stellar Populations of Galaxies, 149, 255. Springer Verlag
Fisher, D., Franx, M., Illingworth, G., 1995, ApJ, 448, 119 (F95)
Franx, M., Illingworth, G., 1988, ApJ, 327, L55 (FI88)
Gerhard, O. E., 1993, MNRAS, 265, 213

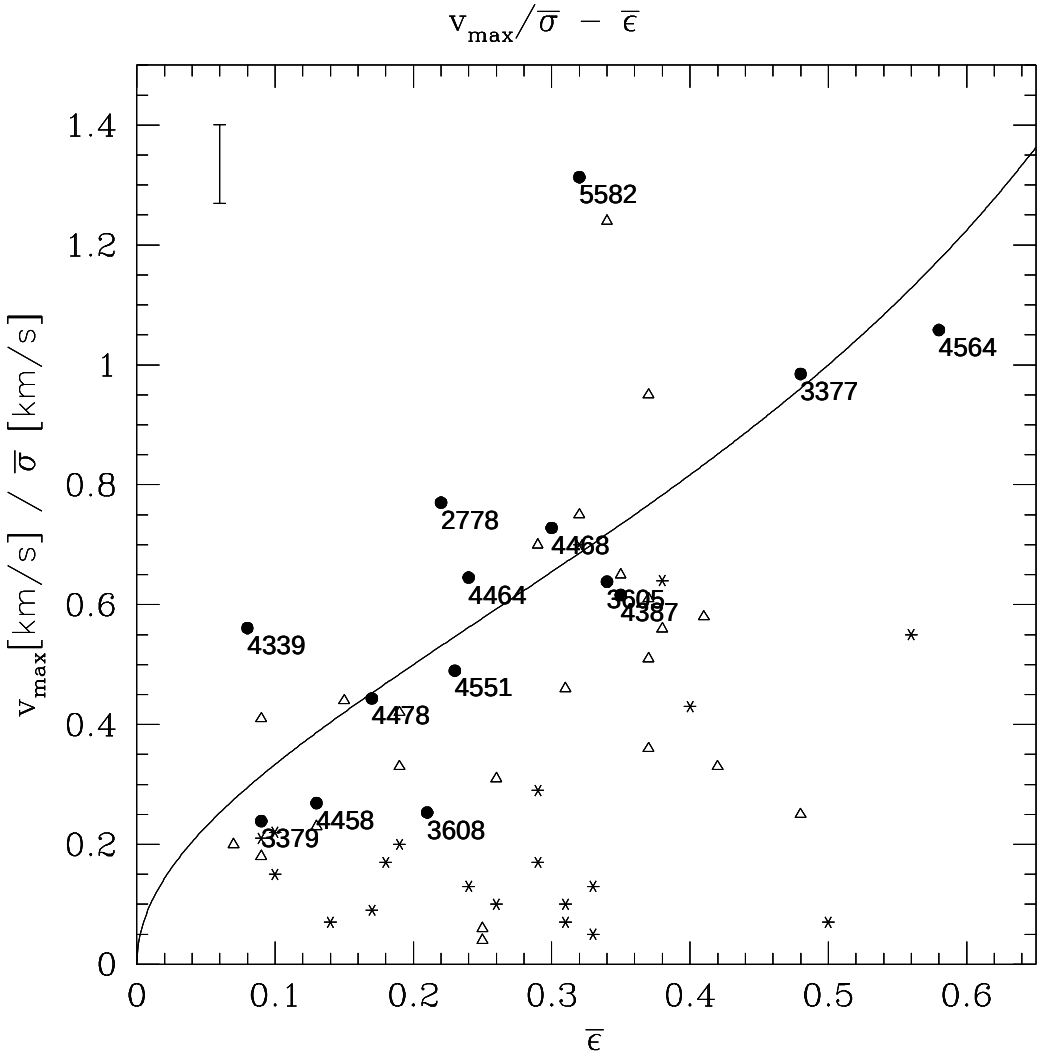

Figure 2. Comparison of measurements of v_{max} / $\overline{\sigma}$ against the mean ellipticity $\overline{\epsilon}$, with predictions for oblate isotropic models (Binney 1978, solid line). Measurements for galaxies studied here are indicated by filled circles. A typical error bar for v_{max} / $\overline{\sigma}$ is given in the upper left-hand corner. Additional measurements are from DEFIS83: measurements for giant ellipticals are given by asterisk symbols, and low-luminosity ellipticals are represented by open triangles.

Halliday, C. 1998, Low-Luminosity Elliptical Galaxies. PhD thesis, University of Durham

Jedrzejewski, R., Schechter, P. L., 1988, ApJ, 330, L87 (JS88)

Kormendy, J., Bender, R., Evans, A. S., Richstone, D. 1998, AJ, 115, 1823 (K98)

Kuijken, K., Merrifield, M., 1993, MNRAS, 264, 712

Lauer, T. R., Ajhar, E. A., Byun, Y.-I., Dressler, A., Faber, S. M., Grillmair, C., Kormendy, J., Richstone, D., Tremaine, S. 1995, AJ, 110, 2622 (L95)

Mehlert, D., Saglia, R. P., Bender, R., Wegner, G. 1998, AA, 332, 33

Mehlert, D., Saglia, R. P., Bender, R., Wegner, G. 2000, A&AS, 141, 449

Peletier, R. F., Davies, R. L., Illingworth, G. D., Davis, L. E., Cawson, M., 1990, AJ, 100, 1091 (P90)

Prugniel, P., Nieto, J.-L., Simien, F. 1987, AA, 173, 49

Rix, H. W., White, S. D. M., 1992, MNRAS, 254, 389 (RW92)

Rix, H. W., Carollo, C. M., Freeman, K. 1999, MNRAS, 513, L25

Saglia, R. P., Kronawitter, A., Gerhard, O. E., Bender, R., 2000, AJ, 119, 153

Sandage, A., Tammann, G. A., 1987, A Revised Shapley-Ames Catalog of Bright Galaxies. Carnegie Institute of Washington (RSA)

Sargent, W. L. W., Schechter, P. L., Boksenberg, A., Shortridge, K., 1977, ApJ, 212, 326

Scorza, C., Bender, R. 1995, AA, 293, 20 (SB95)

Statler, T. S., Smecker-Hane, T., 1999, AJ, 117, 839 (SSH99)

Tonry, J., Dressler, A., Blakeslee, J. P., Ajhar, E. A., Fletcher, A. B., Luppino, G. A., Metzger, M. R., Moore, C. B., 2001, ApJ, 546, 681.

Tonry, J., Davis, M., 1979, AJ, 84, 1511

Trager, S. C., Worthey, G., Faber, S. M., Burstein, D., González, J. J., 1998, ApJS, 116, 1

van den Bosch, F. C., Ferrarese, L., Jaffe, W., Ford, H. C., O'Connell, R. W., 1994, AJ, 108, 1579 (vdB94)

van den Bosch, F. C., Jaffe, W., van der Marel, R. P. 1998, MN-

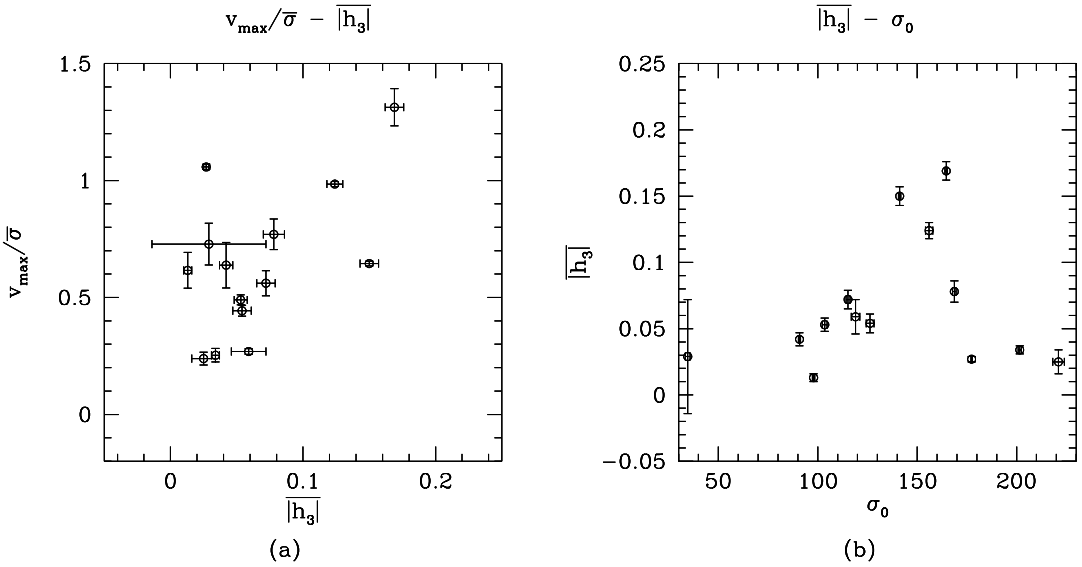

Figure 3. Relationships between global parameters for the major axis of each galaxy. (a) $v_{max}/\overline{\sigma}$ *vs* $|\overline{h_3}|$; (b) $|\overline{h_3}|$ *vs* σ_0. Values of v_{max}, $\overline{\sigma}$ and σ_0 are given in units of km s^{-1}.

RAS, 293, 343
van der Marel, R. P., Franx, M., 1993, ApJ, 407, 525 (vdMF93)
van der Marel, R. P., Rix, H. W., Carter, D., Franx, M., White, S. D. M., de Zeeuw, P. T., 1994, MNRAS, 268, 521 (vdM94a)
van der Marel, R. P., Evans, N. W., Rix, H.-W., White, S. D. M., de Zeeuw, T., 1994, MNRAS, 271, 99 (vdM94b)
Zhao, H. S., Prada, F., 1996, MNRAS, 282, 1223

APPENDIX A: MEASUREMENTS OF GALAXY KINEMATICS

We present our measurements for v, σ, h_3 and h_4 as a function of radius for all galaxies in order of their NGC number.

The systemic velocity of each galaxy was removed by subtracting the mean velocity. Small shifts (<8 km s^{-1}) were applied in order to centre the velocity profile about the apparent kinematic centre of the galaxy. The PA of observation is indicated in each case (values of positive radius correspond to positions in the direction of the PA). Measurements of rotation, σ, h_3 and h_4 obtained for a S/N binning of $\simeq$ 60 per Å are shown by asterisk and open circle symbols for values away from and in the direction of the PA, respectively. Additional measurements for rotation and σ, obtained for a lower S/N binning of $\simeq$ 30-35 per Å, define greater spatial detail and extend to greater radii; these are plotted as open star and open square symbols, away from and in the direction of the PA, respectively. Measurements of rotation and h_3 for radii away from the direction of PA are multiplied by -1 in folding. For some galaxies (NGC 2778, NGC 4339, NGC 4464, NGC 4468, NGC 4478, NGC 5582) the major axis rotation and h_3 measurements are plotted such that the rotation shows mostly positive values.

Where a chromatic focus variation correction for a particular spectrum was applied, this is indicated and the corresponding effective smoothing in arcsec is given. Considerable reference is made to photometry available in the literature, e.g., U, B, and R-band photometry of Peletier et al. (1990, hereafter P90), HST WFPC-1 V-band photometry of van den Bosch et al. (1994, hereafter vdB94) and Lauer et al. (1995, hereafter L95) and HST WFPC-2 V and I-band photometry of Carollo et al. (1997, hereafter C97).

Tables for measurements presented in this appendix are available electronically from the Centre de Donnees astronomiques de Strasbourg (CDS).

A1 NGC 2778

Classified as elliptical in RC3, rotation and velocity dispersion were measured previously for this galaxy by DEFIS83 and F95. Photometry was obtained by P90 who detected a small amount of diskiness for $r \lesssim 7''$, and a gradual isophotal twisting between $3\farcs2$ and $40\farcs1$, from $45\fdg8$ to $42\fdg1$.

For the major axis, h_3 is non-zero for $|r| < 8''$ (see Figure A1). h_4 is positive for $r \sim 7\farcs5$. For the minor axis, h_3 and h_4 are mostly consistent with zero; only at $r \sim 4''$ is a positive h_4 detected.

A2 NGC 3377

A member of the Leo I group, NGC 3377 is widely considered to be a "disky" elliptical. It is classified as an intermediate E5 elliptical galaxy in RC3 and E6 in Sandage and Tammann (1987, hereafter RSA). Photometric measurements by Carter (1987), P90 and Scorza & Bender (1995, hereafter SB95) have shown this galaxy to be "disky" for the range of radii studied here beyond which it becomes "boxy".

For the major axis, h_3 is non-zero for almost all radii. h_4 is mostly consistent with zero (see Figure A2). For the minor axis, h_3 and h_4 are mainly consistent with zero. The rotation curve of the major axis is steeply rising to $\sim$110 km s^{-1} within $r \leq 3''$ and stays roughly constant out to $40''$. The minor axis shows non-zero velocities for $3'' < |r| < 10''$. Our non-zero measurements of h_3 along the major axis are

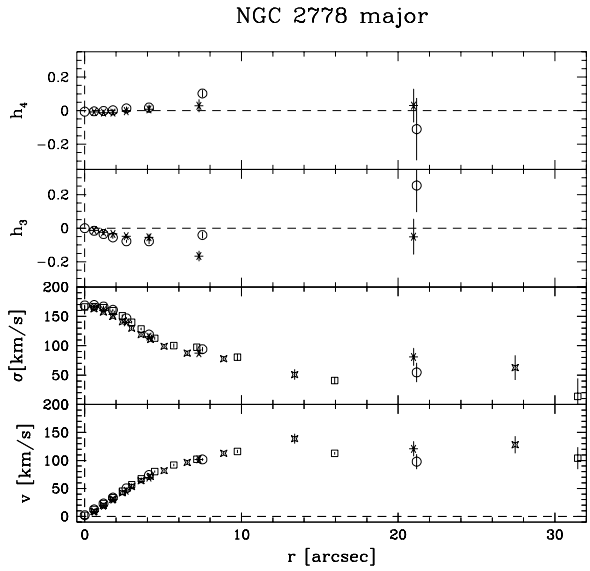

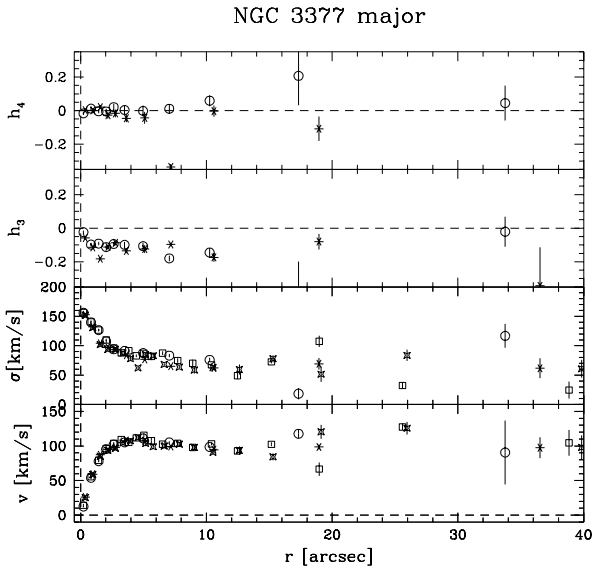

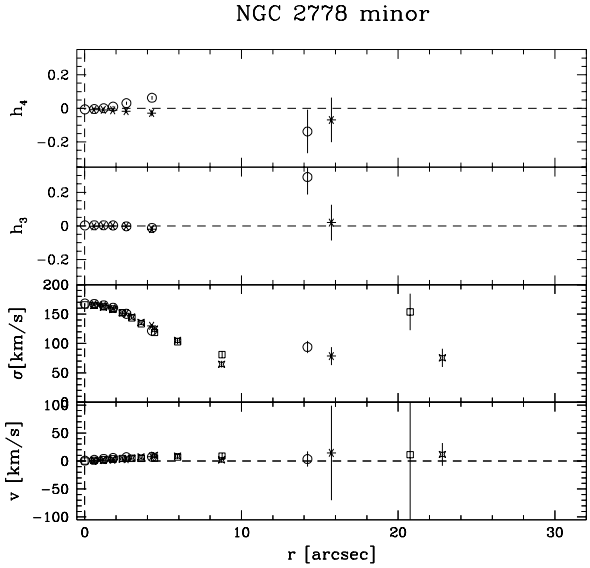

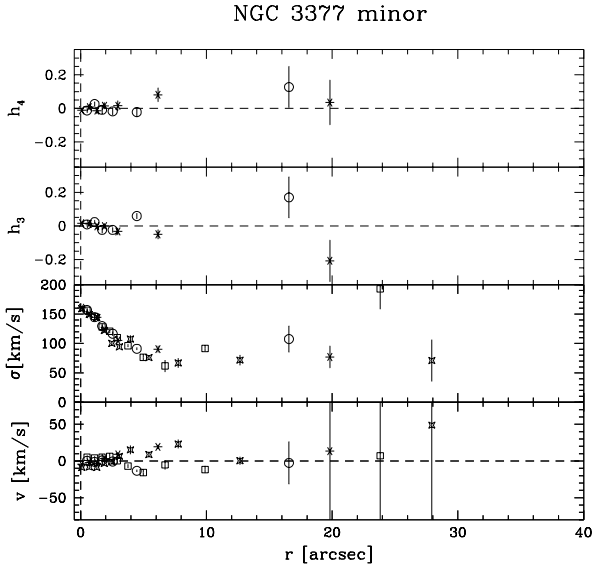

Figure A1. Major and minor axis observations for NGC 2778 (PA 225° and 135°, respectively). Focus corrections were applied for both spectra corresponding to a maximum Gaussian smoothing of 0.″81 and 1.″08, respectively. The seeing for these observations was approximately 1″. The effective seeing, after chromatic focus corrections, is 1.″29 and 1.″47, respectively. Data points cannot be assumed to be independent at this level. In all figures, measurements obtained for a S/N $\simeq$ 60 per Å are presented by asterisk and open circle symbols for values away from the direction of, and in the direction of the PA, respectively. Additional measurements for rotation and σ, obtained for a lower S/N $\simeq$ 30-35 per Å, are plotted as open star and open square symbols, away from and in the direction of the PA, respectively.

Figure A2. Major and minor axis observations for NGC 3377 (PA 42° and 312°, respectively). The seeing for both observations was approximately 0.″8.

consistent with a central disk at radii $|r| < 20''$ as described by SB95.

A3 NGC 3379

NGC 3379 is a member of the Leo-I group and is a well observed elliptical, classified as E1 in RC3.

For the major axis, rotation decreases at $r \sim 4''$ and then increases again at larger radius. Both h_3 and h_4 show small non-zero values but there is no clear trend. For the

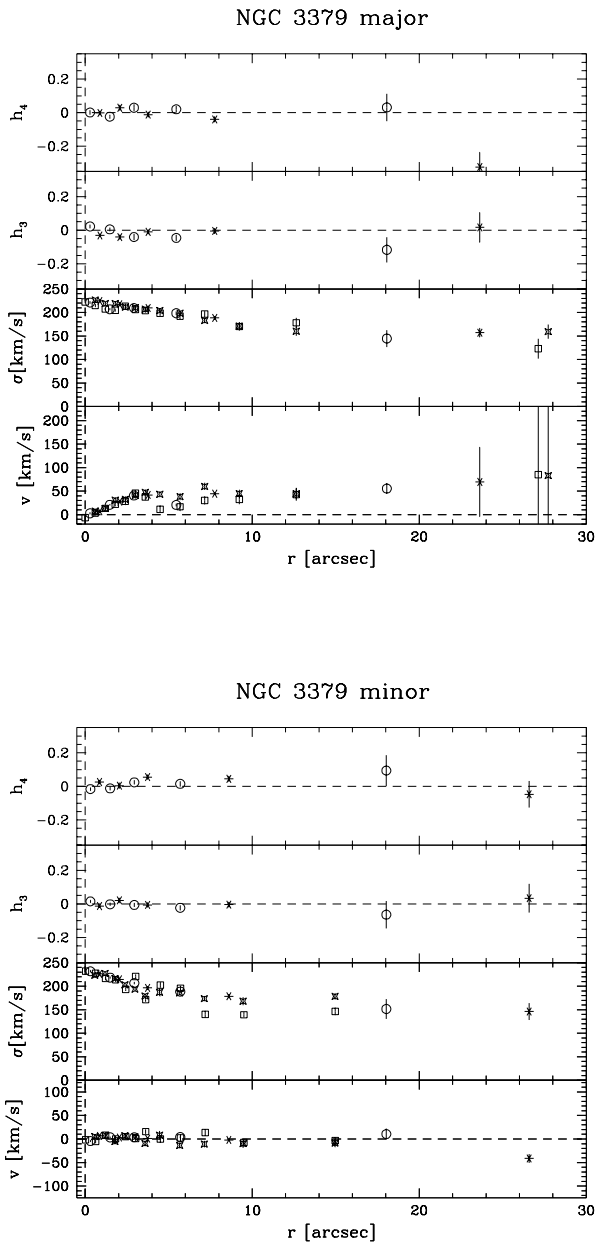

Figure A3. Major and minor axis observations for NGC 3379 (PA 71° and 161°, respectively). The seeing for both observations was approximately 0.″8.

minor axis, both h_3 and h_4 are mostly consistent with zero (see Figure A3).

A4 NGC 3605

NGC 3605, a member of the Leo II group, is classified as an E4 intermediate in RC3, and E5 in RSA. Measurements of rotation and σ for this galaxy were obtained previously by DEFIS83. Photometry for this galaxy was studied by P90 and L95. For $r \lesssim 4''$ the galaxy shows "disky" isophotes while for $r \gtrsim 4''$, the isophotes are increasingly "boxy".

For the major axis spectrum, the most notable features are the non-zero values of h_3 for $2'' < |r| < 7''$ (see Figure A4). h_4 is zero for these radii. For the minor axis, both h_3 and h_4 are consistent with zero close to the galaxy centre, becoming non-zero at greater radii. The minor axis also shows non-zero velocities. It should be noted that the minor axis spectrum was smoothed considerably in the spatial direction in order to account for chromatic focus variations. The non-zero measurement of h_3 for the major axis and the detection of diskiness by L95 at similar radii, support the existence of a central disk component.

A5 NGC 3608

NGC 3608, a member of the Leo II group, is classified as E2 in RC3 and E1 in RSA, this galaxy was one of the first to be recognised to contain a KDC (JS88). The counterrotation of the galaxy core was suggested by JS88 to be the result of an interaction with another galaxy, without full merging, which caused the motion of the outer parts to be reversed. NGC 3608 is one of several KDC candidates imaged by C97. From measurement of the $V - I$ colour gradient, C97 found no significant stellar population differences between the core and surrounding galaxy of NGC 3608. They found the ellipticity increased from a value close to zero at $r \simeq 0.''1$, to $\epsilon \simeq 0.2$ at $r \simeq 4''$, and NGC 3608 to be slightly boxy for radii outside $5''$.

The profiles of h_3 and h_4 for both the major and minor axes, are asymmetric about the galaxy kinematical centre (see Figure A5). A small amount of rotation is detected along the minor axis. The measured velocity along the minor axis for $|r| \gtrsim 10''$ is consistent with zero rotation. Since NGC 3608 has a counterrotating KDC, the LOSVD is likely to be more accurately described by a two-component parameterization.

A6 NGC 4339

NGC 4339 is a member of the Virgo cluster and classified as E0 in RC3 and S0$\frac{1}{2}$ in RSA, this galaxy is intermediate between an elliptical and S0 galaxy.

For this galaxy, the most striking result is a large positive value of h_4 at almost all radii for both, the major and minor axis. For most measurements h_3 is non-zero along the major axis and consistent with zero for the minor axis (see Figure A6).

A7 NGC 4387

NGC 4387 is a member of the Virgo cluster and classified as elliptical in the RC3. This galaxy was one of 8 of the 45 ellipticals imaged by L95, suspected to contain a nuclear star cluster. Such a component was proposed to explain an upturn in the measured surface brightness towards the HST resolution limit.

Both major and minor axis observations show a noticeable dip in σ at the galaxy centre (see Figure A7). For $0'' \lesssim r \lesssim 5''$ along the minor axis, h_4 is slightly positive. For the major axis, h_3 is slightly non-zero for $1.5'' \lesssim |r| \lesssim 5''$ and positive for $r \gtrsim 7''$. h_4 is positive for $r \lesssim -5''$. Outside

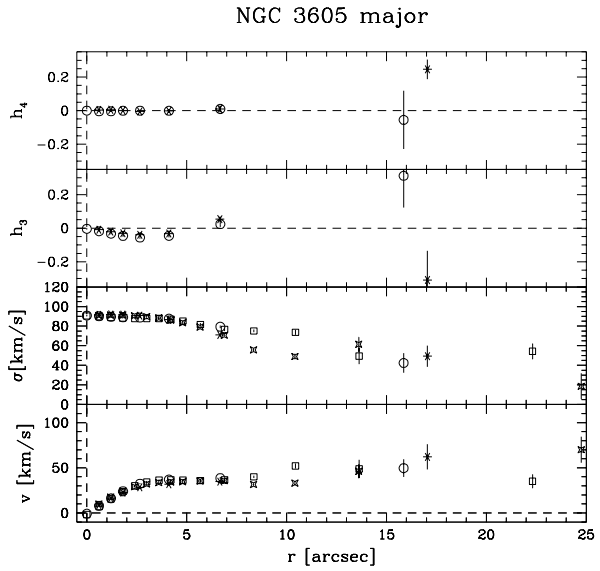

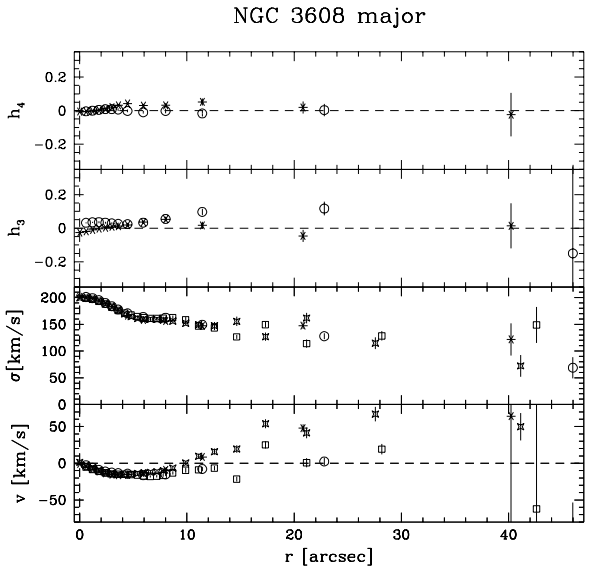

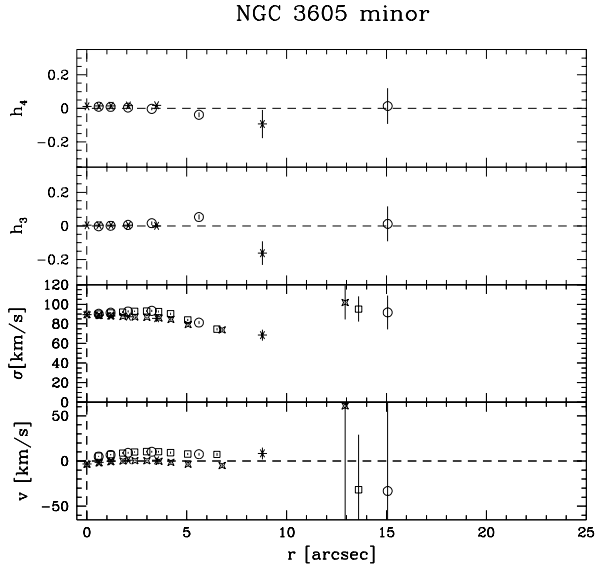

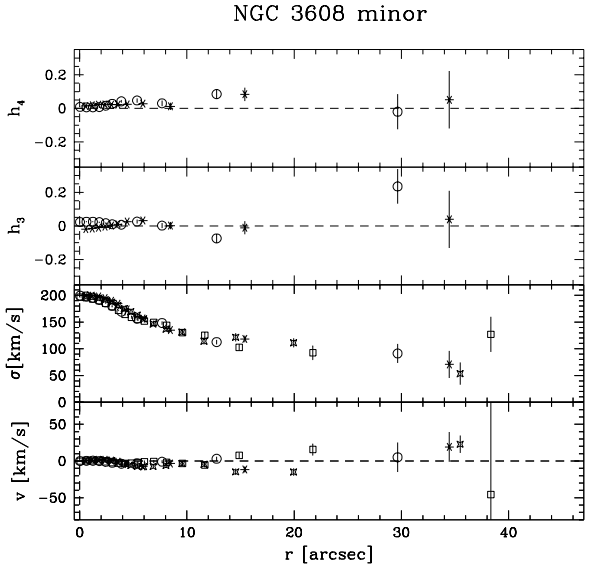

Figure A4. Major and minor axis observations for NGC 3605 (PA 290° and 200°, respectively). The minor axis observation was subject to significant smoothing during focus corrections, i.e. a maximum Gaussian smoothing of 1.″44 was applied. For the major axis spectrum, a maximum smoothing of 0.″69 was required. The seeing for both observations was ∼1″; the total effective smoothing in the spatial direction is therefore 1.″75 and 1.″21 for the minor and major axis observations, respectively.

Figure A5. Measurements for major and minor axes of NGC 3608 (PA 81° and 351°, respectively). Focus corrections were applied for both spectra corresponding to a maximum Gaussian smoothing of 0.″99 in both cases. The seeing was approximately 1″ for both spectra. The total smoothing in the spatial direction was therefore ∼1.″5.

∼ 4″ this galaxy was observed by P90 to have predominantly boxy isophotes.

The central decrease in σ for both axes suggests that a separate, more rotationally supported component is present at the galaxy centre.

A8 NGC 4458

NGC 4458 is a member of the Virgo cluster and is classified as an E0 intermediate elliptical galaxy in RC3. Studied by L95, its ellipticity was measured to decrease from a value of ∼ 0.5 at r ∼0.″5 to close to zero at r ∼7.″5.

Our velocity measurements along the major axis show a clear signature of a KDC within $|r| < 5''$ and a maximum rotation speed of ∼30 km s^{-1}(see Figure A8). At radii $|r| >$

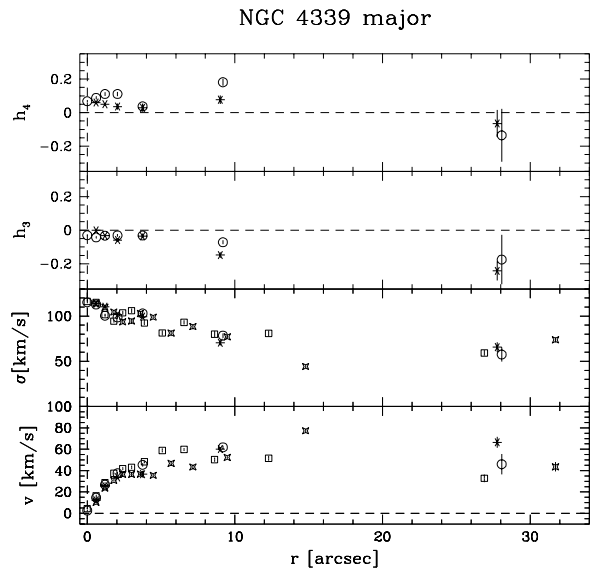

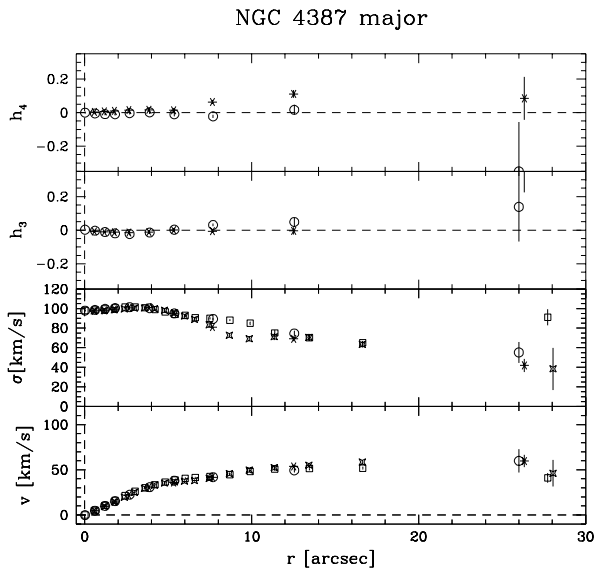

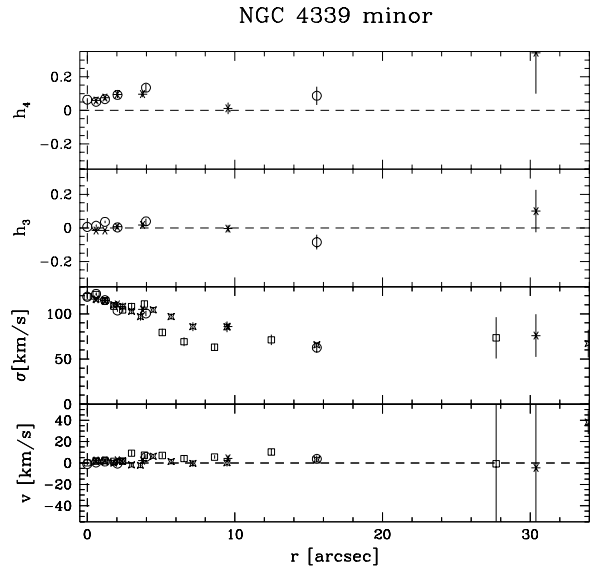

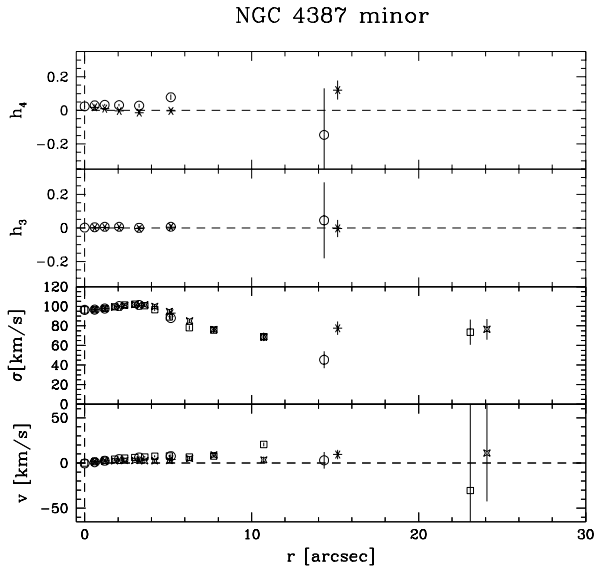

Figure A6. Major and minor axis observations for NGC 4339 (PA 20° and 110°, respectively). Focus corrections applied to both spectra were small with 0.″65 and 0.″50, respectively. The seeing for both observations was approximately 0.″5. Major axis measurements of rotation have been multiplied by -1 for display purposes.

Figure A7. Major and minor observations for NGC 4387 (PA 142° and 52°, respectively). Focus corrections corresponding to smoothing of 0.″86 and 0.″76, respectively, were applied. The seeing for both observations was $\sim 1''$; the total effective smoothing in the spatial direction is therefore 1.″32 and 1.″26.

$5''$ we do not detect any significant rotation. The profiles for both h_3 and h_4 are very unusual and change sharply between independent points. h_4 is measured to be slightly negative close to the galaxy centre for both axes. For radii in the direction of the observation PA, h_3 is positive for the major axis, and the minor axis outside the galaxy centre, and is slightly negative for small negative radii on the major axis.

A9 NGC 4464

NGC 4464 is a member of the Virgo cluster and has an uncertain classification as a spiral galaxy in RC3. Observed by L95, a_4 was measured to be almost zero for the central $4''$, and ellipticity $\epsilon \sim 0.35$ for $1'' \lesssim r \lesssim 10''$.

For radii $|r| \lesssim 10''$ along the major axis, significant asymmetrical and symmetrical deviations of the LOSVD from a Gaussian are indicated by non-zero h_3 and h_4 (see Figure A9). The measurements of h_4 are of large amplitude

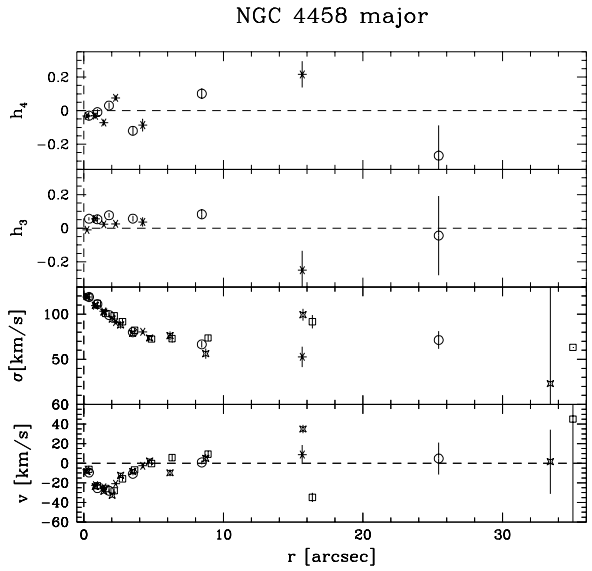

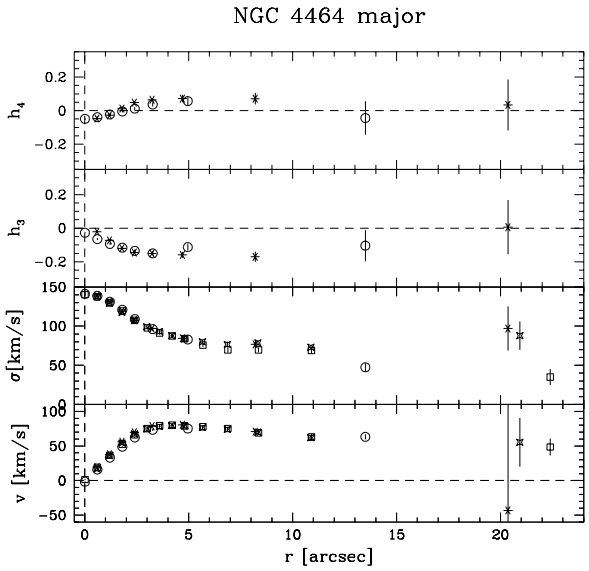

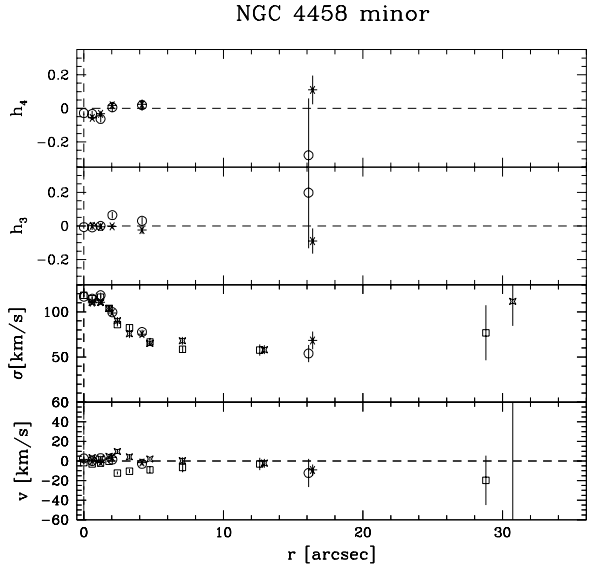

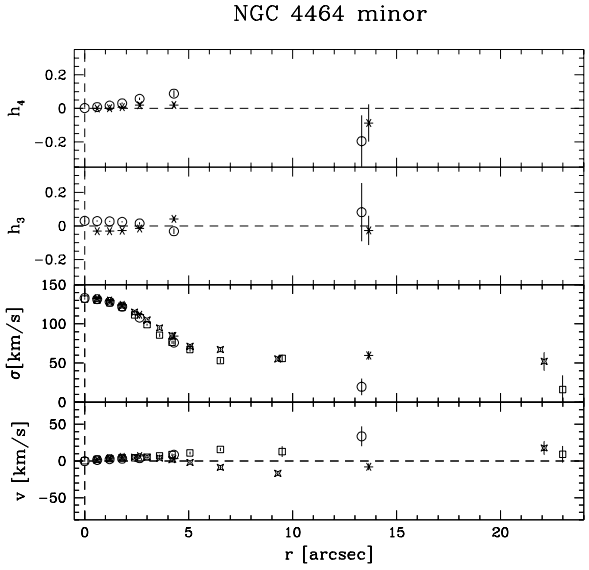

Figure A8. Major and minor axis observations for NGC 4458 (PA 5° and 95°, respectively). The seeing for both observations was approximately 0.″8.

Figure A9. Major and minor axis observations for NGC 4464 (PA 5° and 95°, respectively). Focus corrections applied to both spectra were 0.″61 and 0.″75, respectively. The seeing for both observations was ∼1.″0. Measurements are therefore independent only on spatial intervals greater than ∼1.″25. Major axis measurements of rotation have been multiplied by -1 for display purposes.

and change sign with increasing radius. The large amplitude of h_3 for the major axis suggests the presence of multiple components of different kinematics along the line-of-sight. For $|r| \lesssim 5''$, the measurements are consistent with the superposition of a bulge and an additional, more rotationally supported, component. At greater radii, the rotation begins to decrease suggesting that the more rotationally supported (perhaps disk) component has a scale-length of $\sim 5''$, and that at $|r| > 5''$ a more slowly rotating bulge component begins to dominate the galaxy light. We note that the kinematic measurements for this galaxies are similar to those of NGC 5582.

A10 NGC 4468

NGC 4468 is a member of the Virgo cluster and has an uncertain classification as S0 in the RC3. Our exposures for the major and minor axes of NGC 4468 were too short to provide good spatial detail for the LOSVD higher order terms. Taking our errors into account h_3 is almost entirely consistent with zero for both the major and minor axes. h_4

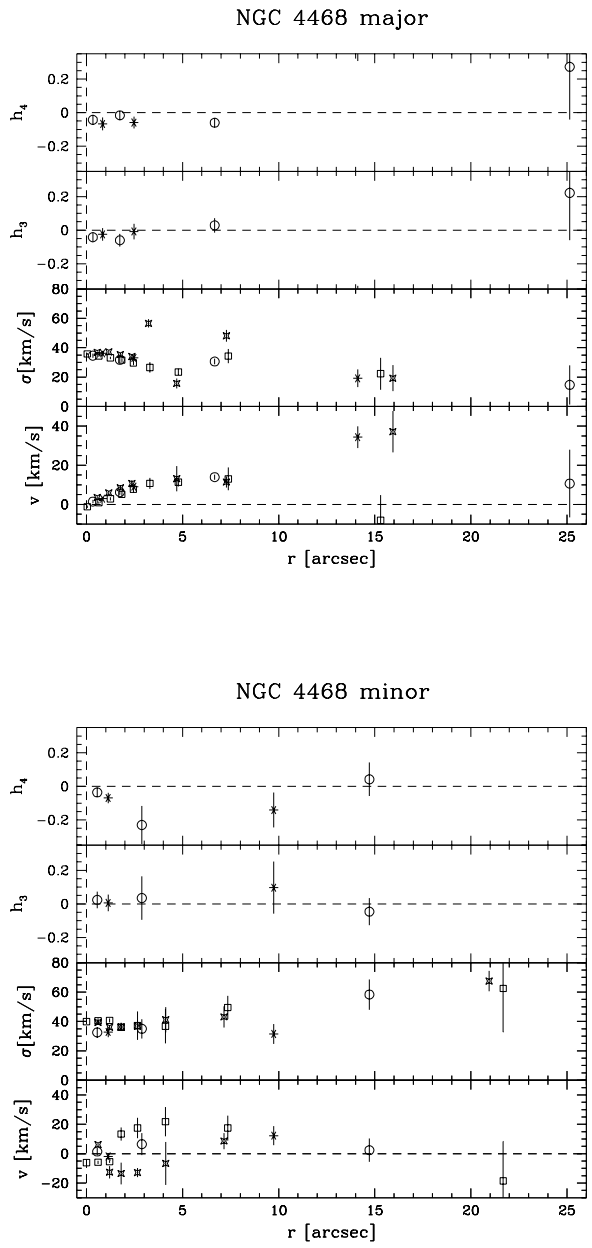

Figure A10. Major and minor axis observations for NGC 4468 (PA 65° and 155°, respectively). The seeing for both observations was approximately 1″. Major axis measurements of rotation have been multiplied by -1 for display purposes.

shows negative values for both major and minor axis (see Figure A10).

Probably a low surface brightness dwarf elliptical or S0 galaxy, the measured rotation and velocity dispersion for this galaxy are very low, with v/σ ∼1.0. These measurements mark the limits achievable for the spectral resolution of our data.

A11 NGC 4478

NGC 4478 is a member of the Virgo cluster. While classified as E2 in both RC3 and RSA, this elliptical is classified as a compact elliptical by Prugniel et al. (1987). They argue that NGC 4478 had been tidally-truncated by its nearby neighbour M87. NGC 4478 has been studied with HST by vdB94. In Figure A12 we show their measurements along the major axis of ϵ, PA and a_4 (kindly supplied by F.C. van den Bosch). Also shown are the measurements of ϵ and PA taken from P90.

In Figure A11, measurements of rotation, σ, h_3 and h_4 for $|r| < 10''$, provide strong indications of a central component, decoupled from the surrounding galaxy. Measurements of σ and h_4 for this range of radii, are asymmetric, and rotation and h_3 are not point-symmetric about the galaxy centre, most notably along the major axis. This could be the result of considerable isophote twisting measured by vdB94 for $|r| < 5''$, such that the measured PA deviated by up to 10° from that of our major axis observation (i.e., PA 145°) (see Figure A12). Observations obtained for the photometric axes of the main galaxy may not therefore coincide with the similar axes of a distinct component. A central decrease in σ is measured for both, minor and major axes. For the major axis, a significantly non-zero value of h_3 is measured for $|r| < 5''$, and h_4 is positive for $0 \lesssim r \lesssim 3''$. For the minor axis, h_3 is slightly non-zero for $|r| < 2''$, and h_4 becomes slightly negative outside $r = 3''$.

Two additional interesting features of the photometry of vdB94 (Figure A12) are the significant measurement of diskiness for the inner 2″ and the sharp increase in ellipticity for $|r| \lesssim 1.5''$. These two results offer strong support to the idea that a disk component resides at the galaxy centre. From the study of residual maps of their photometry, vdB94 were unable, however, to state conclusively that such a component was observed.

The asymmetric LOSVDs along the major axis (i.e., non-zero measurement of h_3) together with the positive measurement of h_4 for both axes close to the galaxy centre, are consistent with the detection of a separate kinematical component with orbital motion across the line-of-sight. The central dip in σ, for similar radii, suggests that this component is more rotationally-supported than the surrounding bulge component. Taken together these results may be consistent with the detection of a central disk population.

The kinematics of this galaxy are clearly complex. Two-dimensional maps of the velocity field, available using integral field unit spectroscopy, would greatly enhance the study of its dynamics.

A12 NGC 4551

NGC 4551 is a member of the Virgo cluster and has an uncertain classification as elliptical in RC3. Our kinematic measurements are presented in Figure A13. This galaxy was studied by both, P90 and L95. The photometric measurements of L95 found NGC 4551 to have "disky" isophotes for $1'' \lesssim |r| \lesssim 4''$. As for NGC 4387, L95 have postulated that NGC 4551 may contain a central stellar nucleus. P90 measure NGC 4551 to become increasingly "boxy" from $r \sim 4''$ to $r \sim 10''$, and at greater radii a_4 tends to zero.

For the major axis h_3 is non-zero for $|r| \lesssim 5''$. h_4 shows

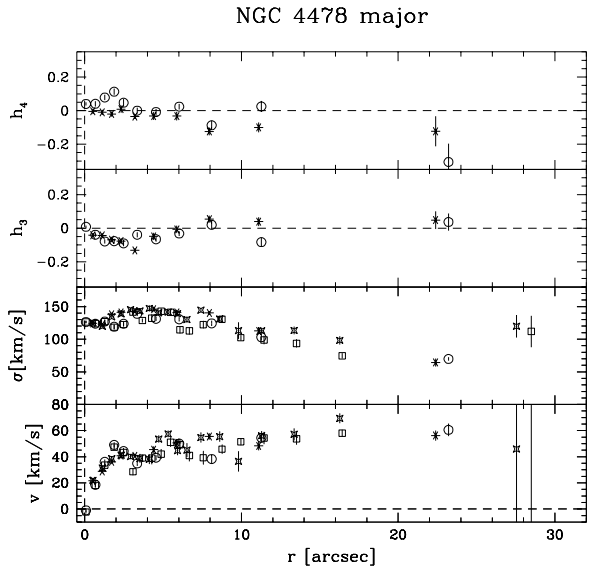

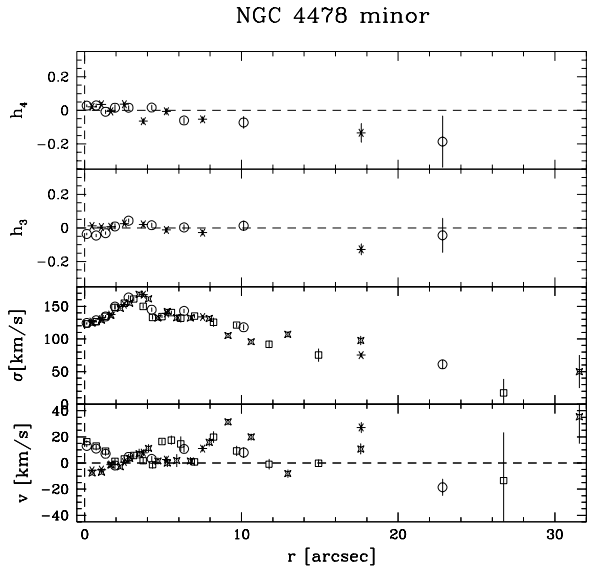

Figure A11. Major and minor axis observations of NGC 4478 (PA 145° and 55°, respectively). The seeing for observations was approximately 0.″8 and 0.″5, respectively. Major axis measurements of rotation have been multiplied by -1 for display purposes.

non-zero values close to the galaxy centre. For the minor axis h_4 changes only slightly with radius and is almost consistent with a value of zero.

Rotation is measured for the major axis and no rotation is detected for the minor axis. A small central decrease in σ is clearly observed for the minor axis. For the major axis this effect is less pronounced. The dip in central velocity dispersion and the measured LOSVD asymmetry for $|r| \lesssim 5''$ along the major axis may be consistent with the detection of a distinct central component of orbital motion across the line-of-sight.

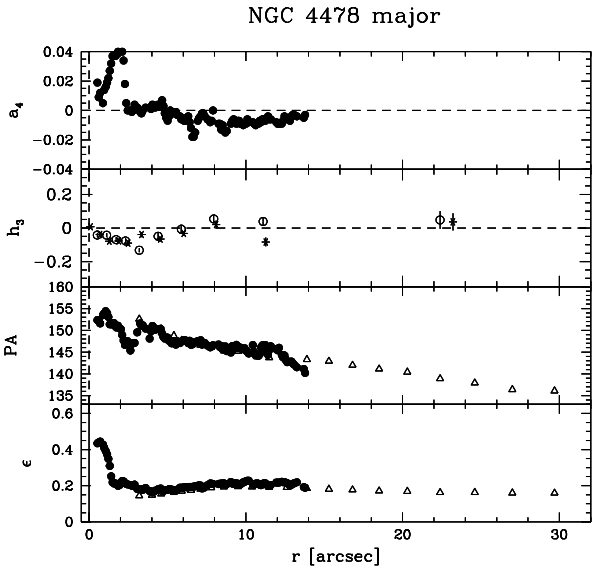

Figure A12. Our measurements of h_3 for the major axis of NGC 4478, are shown along with photometric measurements of ϵ, PA and a_4 from the literature; vdB94 filled circles, P90 open triangles. Measurements of h_3 have been folded by multiplying measurements for negative values of radius by -1.

A13 NGC 4564

NGC 4564 is a member of the Virgo cluster and classified as E6 in both RC3 and RSA. Measurements of v, σ, h_3 and h_4 are given in Figure A14. This galaxy has been studied by vdB94 using HST photometry and in Figure A15 major axis measurements of h_3 obtained here are compared with the photometric measurements of ϵ, PA and a_4 from vdB94.

Non-symmetric LOSVDs are detected along the major axis by non-zero h_3 for $|r| \gtrsim 5''$. h_4 is consistent with zero. For the minor axis h_3 is non-zero for $-9'' \lesssim r \lesssim -5''$ and $r \sim 9''$. h_4 is positive for $|r| \geq 5''$.

In Figure A15, the most interesting results from the photometry are the measurement of negative a_4 and hence boxiness for $r \sim 2''$, and measurement of diskiness for $|r| \gtrsim 10''$, isophote twisting for $r < 2.''5$, and gradually increasing measurement of ϵ with radius. The measurements of a_4 for different radii suggest that two separate components are being detected: within the inner $6''$ the measurements of boxy isophotes are consistent with existence of a central bulge; diskiness for $r \gtrsim 10''$, where rotation is still measured to increase with radius, and the gradual increase in ϵ with radius, are consistent with the detection of a disk component. Measurements are consistent with detection of a disk component embedded within a more slowly rotating bulge.

A14 NGC 5582

NGC 5582 is classified as elliptical in RC3. Measurements are presented in Figure A16. For the major axis, h_3 is significantly non-zero for $|r| < 14''$ and reaches a maximum amplitude for radii at which there is a knee in the rotation curve. h_4 changes significantly in value with radius. For the

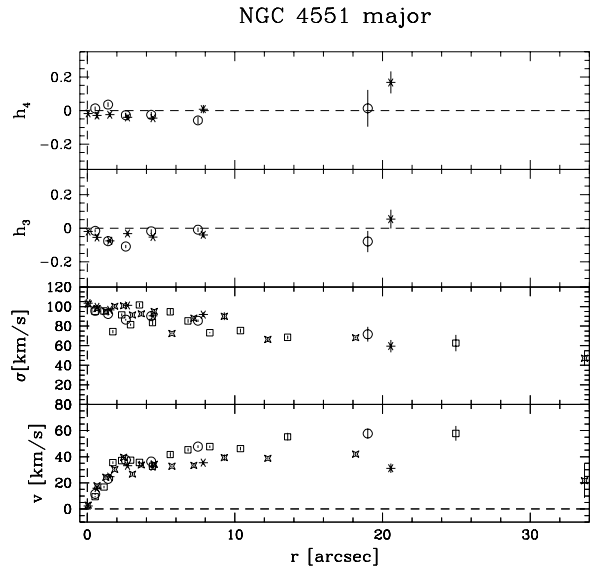

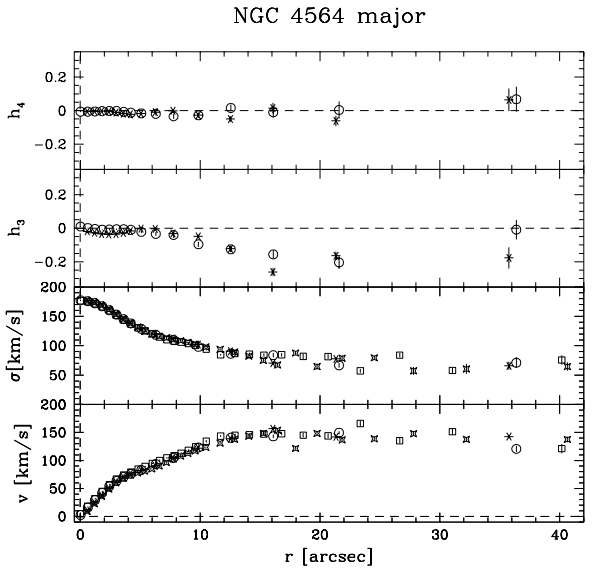

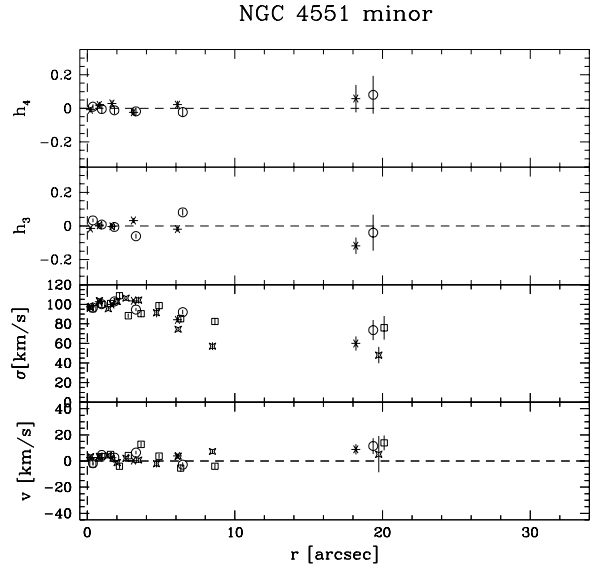

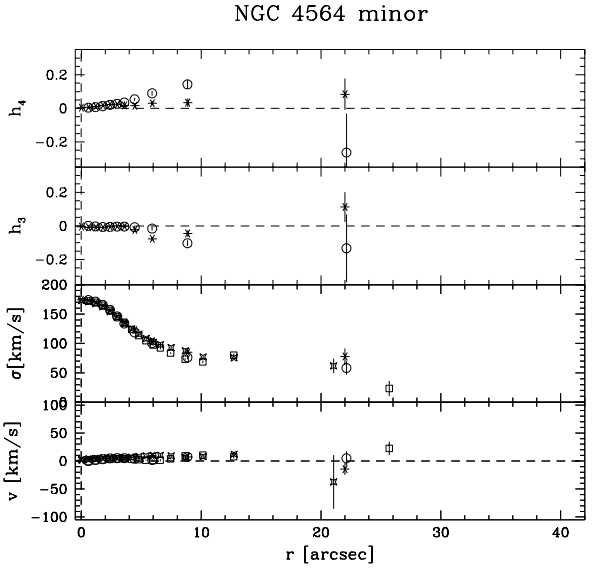

Figure A13. Major and minor axis observations for NGC 4551 (PA 70° and 160°, respectively). The seeing for both observations was approximately 0.″8.

Figure A14. Measurements for the major and minor axes of NGC 4564 (PA 45° and 135°, respectively). Both spectra were corrected for the effects of focus variations; the maximum smoothing applied, 0.″82 for the major axis spectrum, and 0.″74 for the minor axis spectrum, was in both cases smaller then the seeing of $\sim 1''$. The total effective smoothing is 1.″29 and 1.″24, respectively.

inner $10''$, the measurements closely resemble those for the major axis of NGC 4464.

Examples of actual fits to the recovered galaxy broadening function, i.e. the recovered LOSVD shape, are given in Figure 1 in the main part of this paper. For $r < -1''$, the LOSVD is clearly asymmetric and for $r < -2''$ there is clear evidence for the existence of two separate kinematical components, one of which has greater mean velocity along the line-of-sight and appears to dominate the measured kinematics. This is consistent with detection of a separate bright disk component, or a bulge component of high rotational support.

APPENDIX B: COMPARISONS WITH OTHER AUTHORS

Comparisons are made between measurements of v, σ, h_3 and h_4 obtained here and measurements obtained previously by other authors (BSG94, Kormendy et al. 1998, hereafter K98, and SSH99). Measurements have been obtained for the major axis of NGC 3379, NGC 3377 and NGC 4564

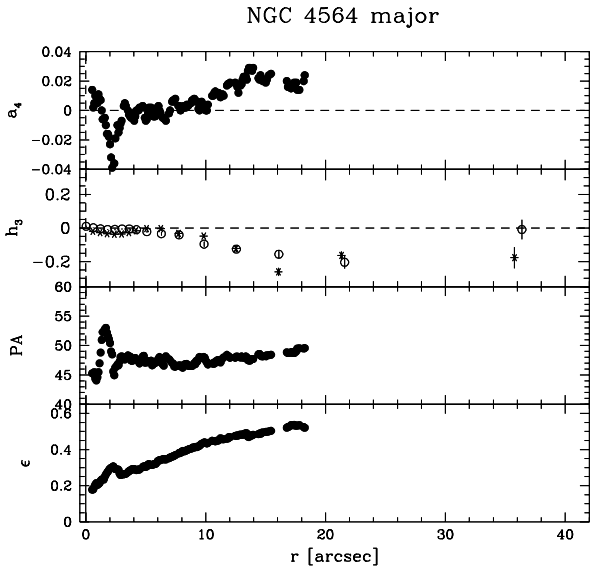

Figure A15. h_3 measurements for the major axis of NGC 4564 obtained here are plotted together with the photometric measurements of van den Bosch et al. (1994) (i.e. measurements of a_4, ellipticity (ϵ) and PA as functions of radius). Measurements of h_3 have been folded by multiplying measurements for negative values of radius by -1.

by BSG94, for the major axis of NGC 3379 by SSH99, and for rotation velocity and σ of NGC 3377 by K98. The PAs of different observations for a given galaxy differed slightly, but in all cases by less than 5°. Results of comparisons are given in Figure B1.

There is in general very good agreement between our measurements and those of other studies. Disagreements can be attributed to the different seeing conditions, instrumental set-ups and exposure times. For NGC 3377 there is remarkably good agreement for the higher-order terms h_3 and h_4. There are however differences in the measurements of rotation and σ at the galaxy centre. The better spatial resolution of our own observations and particularly those of K98 are able to resolve the steeply rising rotation curve; the σ measurements of K98 are also lower for these radii than both our own and those of BSG94, reflecting their improved resolution of the rotation curve. For NGC 3379 our measurements of rotation, σ, h_3 and h_4 agree well with the measurements of BSG94 and SSH99. For NGC 4564, there is disagreement between our measured values of h_3 for $r \gtrsim 12''$ and those of BSG94.

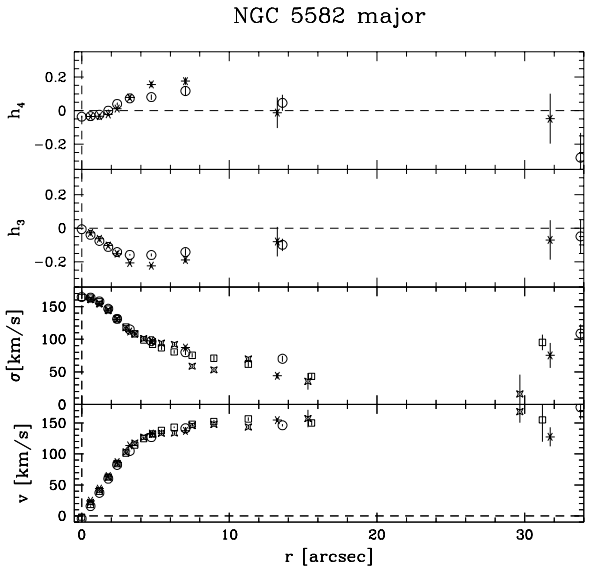

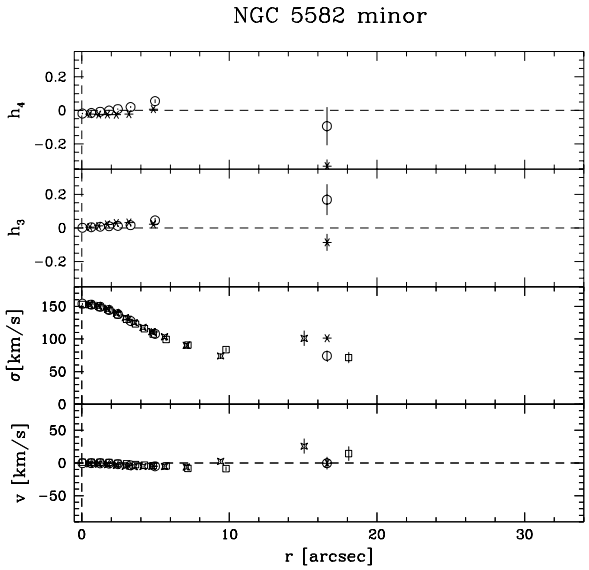

Figure A16. Major and minor axis observations for NGC 5582 (PA 25° and 115°, respectively). Focus corrections applied for the major and minor axis spectra corresponded to a *maximum* Gaussian smoothing of $0\farcs74$ and $1\farcs30$, respectively. The seeing for the minor axis observation was $1''$; measurements for this spectrum can not be assumed to be independent on spatial intervals $\simeq 1\farcs6$.

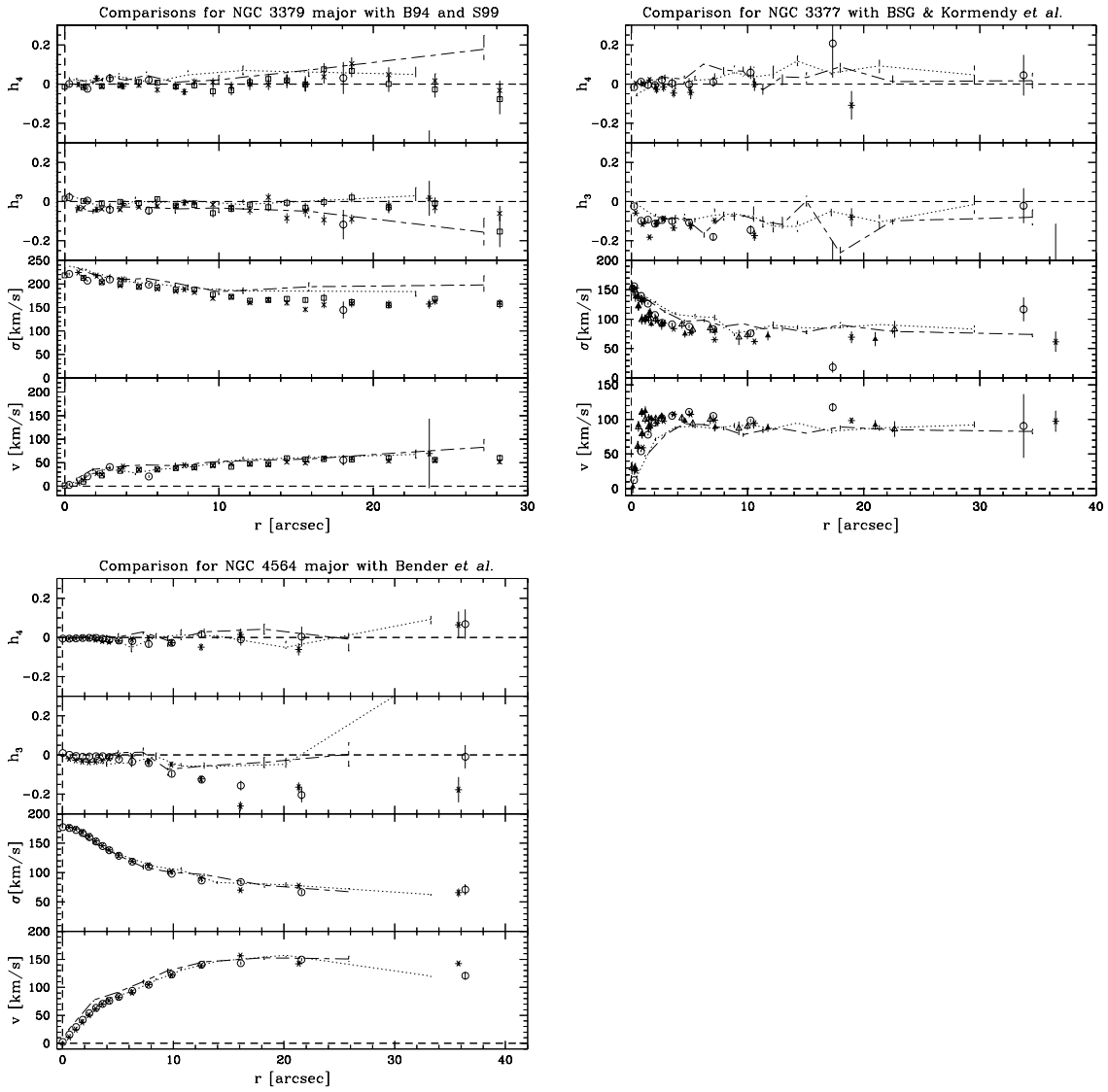

Figure B1. Comparison of measurements of rotation velocity, σ, h_3 and h_4 for galaxies in common with those studied by BSG94, SSH99 and K98. Measurements obtained in this study are indicated by open circles and asterisks for measurements in the direction and away from the direction of the PA of observation, respectively. BSG94 measurements are connected by dot and dashed lines for measurements in and away from the direction of the PA, respectively. SSH99 measurements are given by open and crossed square symbols for measurements in and away from direction of PA. K98 measurements are given by open and solid triangle symbols for measurements in and away from PA direction.